

Annual Review of Analytical Chemistry

Nondestructive 3D Pathology with Light-Sheet Fluorescence Microscopy for Translational Research and Clinical Assays

Jonathan T.C. Liu,^{1,2,3} Adam K. Glaser,^{1,4}
Chetan Poudel,⁵ and Joshua C. Vaughan^{5,6}

¹Department of Mechanical Engineering, University of Washington, Seattle, Washington, USA;
email: jonliu@uw.edu

²Department of Laboratory Medicine and Pathology, University of Washington, Seattle,
Washington, USA

³Department of Bioengineering, University of Washington, Seattle, Washington, USA

⁴Allen Institute for Neural Dynamics, Seattle, Washington, USA

⁵Department of Chemistry, University of Washington, Seattle, Washington, USA

⁶Department of Physiology and Biophysics, University of Washington, Seattle, Washington,
USA

ANNUAL
REVIEWS **CONNECT**

www.annualreviews.org

- Download figures
- Navigate cited references
- Keyword search
- Explore related articles
- Share via email or social media

Annu. Rev. Anal. Chem. 2023. 16:231–52

First published as a Review in Advance on
February 28, 2023

The *Annual Review of Analytical Chemistry* is online at
anchem.annualreviews.org

<https://doi.org/10.1146/annurev-anchem-091222-092734>

Copyright © 2023 by the author(s). This work is licensed under a Creative Commons Attribution 4.0 International License, which permits unrestricted use, distribution, and reproduction in any medium, provided the original author and source are credited. See credit lines of images or other third-party material in this article for license information.



Keywords

computational pathology, digital pathology, optical-sectioning microscopy, spatial biology, precision medicine

Abstract

In recent years, there has been a revived appreciation for the importance of spatial context and morphological phenotypes for both understanding disease progression and guiding treatment decisions. Compared with conventional 2D histopathology, which is the current gold standard of medical diagnostics, nondestructive 3D pathology offers researchers and clinicians the ability to visualize orders of magnitude more tissue within their natural volumetric context. This has been enabled by rapid advances in tissue-preparation methods, high-throughput 3D microscopy instrumentation, and computational tools for processing these massive feature-rich data sets. Here, we provide a brief overview of many of these technical advances along with remaining challenges to be overcome. We also speculate on the future of 3D pathology as applied in translational investigations, preclinical drug development, and clinical decision-support assays.

MOTIVATION FOR 3D PATHOLOGY

For over a century, the gold standard for diagnostic medicine has been based on histopathology, which is the examination of thin tissue sections mounted and stained on glass slides and visualized with an analog brightfield microscope. Conventional histology involves preserving tissue specimens in formalin-based fixatives that degrade nucleic acids, followed by dehydration in chemicals such as xylene and ethanol such that the tissues may be embedded in paraffin wax and thinly sectioned (4–5 microns thick) onto glass slides. Once sectioned, the tissues are most often stained with chromophores such as hematoxylin and eosin (H&E) and occasionally with targeted probes such as antibodies or oligonucleotides (for in situ hybridization). Some negative aspects of this process, as illustrated in **Figure 1**, include (a) destructive sectioning of tissues, which can impede downstream molecular assays that require ample tissue material, (b) severe sampling limitations, in which 1% or less of a tissue specimen is typically sectioned and visualized by pathologists, and (c) the lack of volumetric information, which can result in investigational and diagnostic ambiguities. The digitization of histology slides, known as whole slide imaging, has recently been approved by the US Food and Drug Administration. While this facilitates computational analysis (i.e., artificial intelligence and machine learning), it requires an additional step of scanning slides that does not mitigate any of the challenges of slide-based histology listed above.

Recent technical advances now offer the potential to improve upon the long-standing gold standard of histopathology by imaging thick tissue specimens nondestructively such that 100% of the specimen is maintained for downstream assays. With this technological paradigm, volumetric information about the tissue microarchitecture and molecular constituents can be obtained throughout the entire specimen, which is orders-of-magnitude more tissue than is currently sampled/visualized via conventional two-dimensional (2D) histology sections. The main innovations that have enabled this new field of nondestructive three-dimensional (3D) pathology, which are surveyed within this article, include thick-tissue clearing and labeling strategies to generate fluorescent samples that are highly transparent to light, along with high-throughput, user-friendly 3D microscopy systems in conjunction with advanced data science methods and instrumentation for handling the massive data sets that are generated.

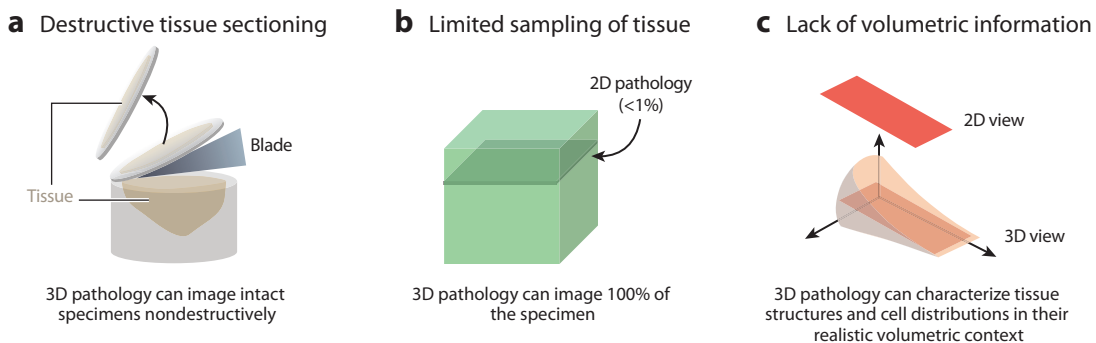


Figure 1

Limitations of two-dimensional (2D) pathology that can be overcome with three-dimensional (3D) pathology. (a) Destructive sectioning of tissues in conventional 2D histology methods can impede downstream molecular assays that require ample tissue material, unlike nondestructive 3D pathology methods. (b) Due to the destructiveness and time-consuming nature of physically sectioning tissues onto glass slides, there are severe sampling limitations for conventional 2D histology. With nondestructive 3D pathology, large specimens can often be imaged in toto, which enables improved diagnostic sensitivity, the ability to identify rare events that are often missed with 2D sections and, most importantly, (c) the ability to accurately characterize complex 3D structures and cell distributions, which can improve investigational and diagnostic certainty.

Downloaded from www.annualreviews.org.

Guest (guest)

IP: 13.58.121.251

On: Tue, 21 May 2024 04:44:04

3D microscopy methods have been available to life scientists for several decades, most ubiquitously in the form of confocal and multiphoton microscopes (1–5), and occasionally through reconstructions of serially sectioned tissue blocks (6–8). Major advances in biological understanding have been gained by such workhorse microscopy techniques in research settings. However, such systems are limited in speed because they are fundamentally laser-scanned imaging techniques in which images are generated in a point-by-point fashion over time. Although various approaches have been developed to improve imaging speed, such as the use of spinning disks for confocal microscopes (9, 10) and temporal focusing or multifocal methods for multiphoton microscopy (11–13), imaging speeds have still precluded the mainstream application of such techniques for high-throughput preclinical or clinical applications.

One area in which conventional optical-sectioning microscopy approaches (e.g., confocal and multiphoton microscopy) offer great advantages is for imaging highly scattering uncleared tissues, as is necessary for *in vivo*/intravital imaging applications. This is because of the background-rejection and background-suppression abilities of confocal and multiphoton microscopy, respectively, which are sacrificed with faster camera-based 3D microscopy techniques such as light-sheet and light-field microscopy. Sophisticated miniaturized forms of confocal and multiphoton microscopes have even been developed to enable endoscopic microscopy within human patients—for surgical guidance or early detection of malignancies—or for long-term neuroimaging in the brains of awake, freely moving rodents, among many other applications (14–19). In this review, we focus on the imaging of *ex vivo* specimens, in which a myriad of clearing and labeling approaches are readily available, and where device miniaturization is not of the highest priority.

We attempt to provide a high-level survey of the following topics pertaining to nondestructive 3D pathology of excised tissues for translational research and clinical diagnostics. (a) We first provide a brief history of light-sheet fluorescence microscopy (LSFM), which has in recent years become recognized as a powerful technique for high-resolution evaluation of large preclinical and clinical specimens that are optically cleared. (b) We present a focused discussion on recent hardware advances and challenges for cleared-tissue LSFM systems. (c) We summarize recent advances in thick-tissue fluorescence labeling and optical clearing. (d) We discuss advances and challenges in raw data processing and image formation. Note that we do not cover downstream image-interpretation and analysis methods, such as deep learning–based denoising, super-resolution, and deconvolution methods, as well as machine-learning methods for image translation (style transfer), image segmentation, and classification. While these topics are highly important and rapidly evolving, they deserve (and have been the subject of) dedicated review articles (20–27). (e) Finally, we provide a forward-looking perspective on future directions for the field of 3D pathology in translational research, preclinical drug development, and clinical-assay development.

BRIEF INTRODUCTION TO LIGHT-SHEET FLUORESCENCE MICROSCOPY

In its basic form, light-sheet microscopy uses spatially localized illumination of a specimen with a thin sheet of light that is designed to coincide with the focal plane of a camera-detection path. Selective illumination in this way is powerful because it enables recording of volumetric images of biological specimens with low background signal, high speed, and minimal photobleaching or phototoxicity (28, 29). In contrast, confocal and widefield microscopes illuminate the entire thickness of a specimen and as a result face drawbacks in speed, background signal, or light dosage.

Although light-sheet microscopy was first used in the early 1900s to study colloids (30, 31), it experienced a boom in popularity starting about a century later when redeveloped for the imaging

of fluorescent biological specimens as LSFM (32, 33). In the past ~20 years, LSFM has been used to study important biological problems including embryonic development (34), cardiac hemodynamics (35), and neural dynamics (36). Many of these studies have been facilitated by highly innovative LSFM instruments, with key advances centered on the choice and arrangement of objective lenses relative to the specimen. These LSFM design innovations can yield significant advantages for specific applications in terms of speed, resolution, range, throughput, cost, and simplicity.

Recent Hardware Advances and Challenges for Cleared-Tissue LSFM Systems

In recent years, there has been considerable effort put into improving the performance and utility of LSFM systems for cleared-tissue imaging. As with most technologies, the pursuit of improved performance for one system specification often results in unavoidable trade-offs. However, state-of-the-art systems strive for an optimal balance in performance, guided by the recent needs of researchers and cleared-tissue imaging experiments (37).

Many of the key design choices for LSFM center on the arrangement of objective lenses; i.e., LSFM systems are often built around the specimen. The original cleared-tissue LSFM design uses two perpendicular objective lenses arranged around a specimen, with a detection objective above or below the specimen, an excitation objective positioned at the side, and the specimen held in place on a substrate, within a cuvette, or within a rotating capillary (**Figure 2a**). While this geometry is relatively simple to implement, it places physical constraints on the lateral size of the specimen such that it is not possible to image large, centimeter-scale tissue slabs or multiple

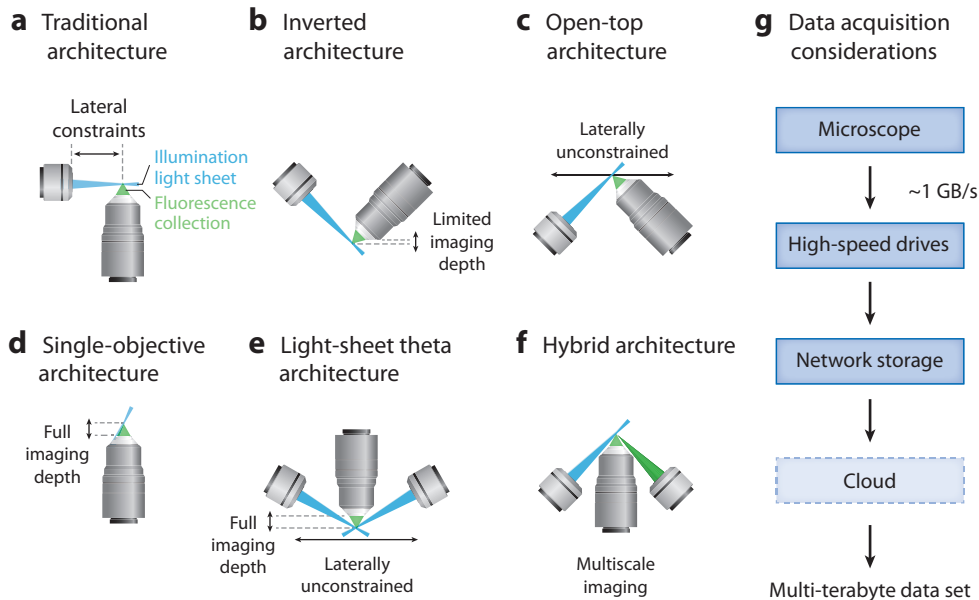


Figure 2

Light-sheet fluorescence microscopy and data handling. (a–f) Architectures of traditional, inverted, open-top, single-objective, light-sheet theta, and hybrid light-sheet microscopy systems. Relevant characteristics of each microscope architecture, including lateral constraints on specimen size and usable imaging depth, are highlighted. (g) Typical data acquisitions associated with any light-sheet microscopy system are listed. These include raw data generation from the microscope itself at ~1 GB/s, storage of the data on high-speed drives, transfer of the data sets to network storage, and optional storage of these often multi-terabyte data sets in the cloud (dotted box).

specimens mounted in standard holders (e.g., well plates). Alternatively, the specimen may be held on a substrate with the perpendicular objective lenses each oriented at an angle relative to the substrate. Positioning both of the objective lenses on the sample side (**Figure 2b**) minimizes optical aberrations but can constrain sample geometries (38–44). Positioning both of the objective lenses below the sample holder, called open-top light-sheet (OTLS) microscopy (**Figure 2c**), requires some care with sample preparation to avoid optical aberrations but enables laterally unconstrained imaging that is particularly well suited to high-throughput imaging of specimens in a range of formats (40–46). A third group of LSFM designs uses a single objective to both deliver the light sheet and collect the emitted fluorescence. In these systems, the illumination and collection beams share a single objective and are nonorthogonal to one another, requiring a method such as remote refocusing to rectify the imaging plane (47–58) (**Figure 2d**). Orienting the objective in the vertical direction with respect to a horizontal specimen holder makes use of the objective's full working distance and dramatically increases the system's tolerance to refractive-index mismatch (relative to inverted and open-top LSFM systems). Most recently, the light-sheet theta microscopy (LSTM) and hybrid OTLS systems have been developed (46, 59). In LSTM (**Figure 2e**) and hybrid OTLS (**Figure 2f**) systems, a high-numerical aperture (NA) collection objective is oriented in the vertical direction (similar to single-objective systems), and a separate illumination objective is used to deliver the light sheet. These designs possess all the advantages of a single-objective LSFM system, whereas the use of a separate illumination objective provides more degrees of freedom to optimize the system resolution for a desired imaging application.

As with any microscopy method, higher spatial resolution is commonly achieved by using objectives with a higher NA. Higher-NA objectives typically have exceedingly short working distances, which for conventional microscopy methods (i.e., conventional widefield and confocal microscopes) limits the specimen size in only one dimension. However, the dual-objective architecture of LSFM systems results in more severe geometric constraints, where the specimen size is now limited in two dimensions. In addition, for the highest NA objectives, it may not be possible to position two objectives relative to one another for LSFM imaging due to the physical dimensions of the objectives themselves. Additional spatial resolution improvements under exploration include incorporation of structured illumination, stimulated emission depletion, and deep learning-based techniques, although all these methods are yet to become mainstream in cleared-tissue LSFM systems (60–63).

Although the previously mentioned approaches are primarily concerned with lateral resolution, there has been equal if not greater interest in improving the axial resolution of an LSFM system. Unlike conventional microscopy methods, the use of a dedicated excitation optical path provides more degrees of freedom that can be optimized to provide improved resolution in the axial dimension (i.e., engineering the light sheet). The majority of LSFM systems use Gaussian beam illumination, which introduces a fundamental trade-off. The Gaussian light sheet is either tightly focused (high axial resolution) yet short and unable to cover the field of view of the system or weakly focused (low axial resolution) but long, providing full coverage of the system's field of view. To overcome this trade-off, strategies have been developed for tiling or axially sweeping a tightly focused light sheet across the field of view (64, 65). Tiling methods discretely step the light sheet across the field of view, capture a separate image for each position, and computationally fuse the overlapping portions of each image together, yielding a single image with high axial resolution across the field of view. One drawback to this approach is decreased imaging speed (multiple image exposures are required for each position with a specimen). Axial sweeping methods overcome this drawback. Rather than discretely stepping the light sheet across the field of view, the light sheet is continuously moved, in sync with the rolling shutter of the camera, which acts as a moving slit, rejecting thick areas of the light sheet and exposing pixels to only the tightly focused portion of

the light sheet. Although axial sweeping requires only one image exposure, the optomechanical elements currently used for axial sweeping can still limit imaging speeds. Additional approaches include the use of non-Gaussian light sheets such as Bessel, Airy, and optical lattices (66–69). These illumination strategies may improve axial resolution, but they can result in reduced image contrast or require computationally expensive deconvolution methods to recover improved performance (70–72).

Although the highest spatial resolution is always desirable, it is worth noting that for any volumetric imaging modality, data set sizes and imaging times typically scale with the cube of the spatial resolution (73). Therefore, large gains in efficiency can be achieved by employing multiscale imaging strategies. For example, an efficient multiscale imaging workflow can be achieved by first using a low magnification system to screen specimens and identify regions of interest, followed by detailed inspection of those small regions of interest using a higher-magnification system. Similar to other microscopy methods, the simplest multiscale implementation is the use of a turret of multiple objectives with varying magnifications. This approach has been demonstrated with several of the previously mentioned LSFM architectures, including the original cleared-tissue design, as well as a recently published multiresolution OTLS system (44). Alternatively, multiple LSFM systems with different magnification set points can be used. In a third approach, a single system can be designed with multiple imaging paths, such as the recently published hybrid OTLS system (46). Finally, some approaches can leverage a single lens to simultaneously provide high resolution and a large field of view (74). These lenses, with a so-called high space-bandwidth product, may be combined with high-megapixel-count cameras to provide multiscale imaging. Regardless of the imaging application or multiscale imaging approach, the spatial resolution of an LSFM system is often chosen to be just enough for the given scientific question and imaging experiment.

Recent Advances and Challenges in Data and Image Processing

LSFM data sets are notoriously challenging to work with. The difficulties begin at the time of acquisition. Unlike many other microscopy methods, LSFM systems generate data at the maximum data rate of the camera [~ 1 GB/s for state-of-the-art scientific complementary metal-oxide-semiconductor (sCMOS) cameras]. For LSFM systems using multiple cameras, the aggregate acquisition rate can quickly reach multiple GB/s (75, 76). To robustly capture this flood of information, specialized considerations must be made to the downstream hardware and software.

Data sets must be streamed to high-speed, solid-state drives or traditional hard disk drives that can be aggregated together as a redundant array of independent disks (RAID) to achieve high write speeds. However, the size of these arrays is often limited to tens of terabytes at most, which is often too little space to store LSFM data sets. Therefore, data sets must often be transferred from a local acquisition workstation to some form of larger networked storage, where the local solid-state drives act as a temporary cache. To prevent this local cache from overflowing, the network transfer speeds must exceed the LSFM system's acquisition speed. High-speed networking at speeds of 10, 40, or even 100 GB/s may be necessary. This requires significant testing and investment from an institution to provide the proper information technology infrastructure to support these high-speed data transfers (77). It is important to note that bandwidth requirements can be reduced by performing online compression. However, the compression algorithm's speed must ideally outpace the LSFM system's acquisition speed (78, 79).

Once an entire data set has been successfully captured, the data must then undergo a number of processing steps. For cleared-tissue experiments, the first step is to register and align the many adjacent imaging tiles resulting from the serial acquisition of those volumetric tiles across a given specimen. Several commercial software packages (such as Imaris Stitcher) as well as popular

Downloaded from www.annualreviews.org.

Guest (guest)

IP: 13.58.121.251

On: Tue, 21 May 2024 04:44:04

open-source tools (such as TeraStitcher, BigStitcher, Bigstream, and Stitching Spark) have been developed to address this challenge (80, 81). These alignment methods can be performed with varying levels of complexity, ranging from pure translation of tiles to full affine transformations, to complete nonrigid deformation and alignment. Once the alignment of all tiles has been determined, the data sets are often fused, yielding a single contiguous volumetric data set with blended seams between adjacent tiles. These operations are increasingly computationally expensive and should ideally be tailored to the requirements of a specific imaging data set. These data sets may then be visualized and/or subjected to downstream postprocessing routines. Regardless of the step, care must be taken to parallelize the task across ample computing resources and to optimize the runtime speed to complete the computational task within a reasonable time frame.

RECENT ADVANCES AND CHALLENGES IN TISSUE LABELING AND CLEARING

In parallel with many of the hardware-based innovations described above, recent years have witnessed major breakthroughs in technologies for sample preparation and workflows that enable the imaging of thicker intact specimens, with higher resolution and lower scattering/aberration, along with rich molecular detail. We review several of these developments here, with an emphasis on areas that are particularly relevant for pathology samples.

Traditional workflows for optical microscopy of thick biological specimens have required physical sectioning of the specimen for several reasons. First, nearly all microscopy-based pathology workflows utilize 2D widefield microscopy techniques in which thin sections ($\leq 10\ \mu\text{m}$) are required to produce clean, blur-free snapshots. Second, even workflows that utilize traditional 3D microscopes (e.g., confocal microscopy) rarely image beyond $\sim 100\ \mu\text{m}$ in depth due to the scattering of light by the specimen. Third, the labeling of thick specimens by large exogenous probes (e.g., antibodies) can require weeks or longer for thicker specimens ($> 100\ \mu\text{m}$) due to the slow pace of passive diffusion of probes within a sample. While many powerful studies are performed within these constraints, they lack the ability to garner insights most easily gained by studying larger intact specimens and 3D structures such as glandular networks (82). The past ~ 20 years have seen a flurry of developments that make imaging of thick specimens easier than ever and have helped set the stage for rapid progress in 3D pathology.

Tissue Clearing and Expansion

A plethora of tissue clearing techniques now exist for combating light scattering and refractive aberrations in tissues, thereby enabling the imaging of specimens 1–10 mm in thickness (83–88). The first subset of techniques are hydrophobic or solvent-based clearing methods that use dehydration and immersion of specimens in various organic solvents in order to reduce the variations in the index of refraction that lead to scattering of light and aberrations. The second subset of techniques uses infusion of aqueous or hydrophilic solutions containing solutes including various sugars or alcohols. Example solvent-based clearing techniques include the DISCO family of methods and ECI, while example aqueous-based clearing techniques include SeeDB, FRUIT, and CUBIC (84, 86, 89–92). A third and somewhat distinct group of clearing techniques, such as CLARITY, synthesizes within the specimen an acrylamide-based hydrogel polymer that serves as a scaffold to hold proteins and some other structures in place while allowing lipids to be removed and enabling infusion of an index-homogenizing solution (87). All of these clearing procedures differ substantially in key properties including complexity, compatibility with different types of fluorescent labels, and the final index of refraction. For instance, Tanaka et al. (93) used iDISCO for tissue clearing of various formalin-fixed, paraffin-embedded human tumors to study

epithelial-to-mesenchyme transition and angiogenesis, whereas Barner et al. (94) used CUBIC-HV for tissue clearing of fresh axillary lymph nodes to assess the ability of 3D pathology to improve breast cancer staging. Impressively, even human organs that are multiple centimeters thick, such as whole kidneys, can be cleared and imaged by light-sheet microscopy, as shown by Zhao et al. (95) using the rapid clearing method, SHANEL (**Figure 3a–d**). SHANEL is based on the use of the detergent CHAPS, which forms small micelles that diffuse more rapidly into tissues than the conventional permeabilization detergents sodium dodecyl sulfate or Triton X-100, in conjunction with *N*-methyl-diethanolamine for decolorization of colorful heme molecules from residual blood clots.

Tissue-hydrogel hybrids have been extensively used in recent years not just for clearing of specimens, but also for physical expansion to enable super-resolution expansion microscopy (ExM) at a resolution of 70 nm or better (96–98). This is achieved in most cases by synthesizing within the sample a polymer composed of sodium acrylate and acrylamide comonomers that links to the sample (87, 99, 100). The resulting tissue-hydrogel hybrid, with its abundant carboxylate groups, has a high osmotic pressure and, when immersed in deionized water, will enlarge to several times its original size. The procedure can be performed with very low distortion and isotropic 3D expansion so that features too close to resolve in the original specimen can be resolved in the expanded state even with lower-resolution microscopes.

Most ExM work to date has been applied to model organisms, but there are notable examples in which it has been used to study human pathology specimens (101, 102). For example, Zhao et al. (101) used ExM to study human kidney biopsy specimens (**Figure 3e,f**), where they were able to accurately distinguish minimal change disease from focal segmental glomerulosclerosis. In current clinical practice, electron microscopy is required to distinguish minimal change disease and focal segmental glomerulosclerosis by examining the nanoscale details of podocyte foot process effacement. ExM already has the potential to become a valuable tool for clinical research and pathology, and as the technology continues to advance at a rapid pace, it is likely to gain even more powerful capabilities in the years to come.

Tissue Labeling

Broadly speaking, fluorescence microscopy uses a rich and ever-growing palette of labels that can provide valuable information about the specimen. Some of the most popular labels used in pathology contexts include antibodies for labeling of specific target proteins, lectins that bind specific carbohydrates, oligonucleotide probes for fluorescence in situ hybridization (FISH) detection of DNA or RNA, and small-molecule labels that relatively nonspecifically bind lipids, DNA, carbohydrates, or proteins.

Although current clinical practice evaluates only thin sections of biopsy tissue (typically $\leq 10 \mu\text{m}$), which requires minimal staining times, the staining of thick specimens with relatively large antibodies (150 kDa, or $\sim 15 \text{ nm}$ across) can be prohibitively slow (e.g., weeks or longer to stain specimens $> 1 \text{ mm}$), and there has been considerable innovation to efficiently deliver antibodies to thick tissues for 3D imaging. Chung and coworkers (87), in particular, have developed several methods to speed up antibody (or other probe) labeling reactions in tissue-gel specimens. SWITCH (103) used a two-step approach in which probes are first delivered in a buffer containing a detergent that prevents probe binding. The probes are then activated in a second buffer without detergent that enables binding. This approach enables decoupling of the rates of probe diffusion and binding and leads to more uniform staining of thick specimens. In a creative use of tissue-gel hybrids called ELAST, Ku et al. (104) synthesized a highly elastic hydrogel within tissue specimens so that antibodies and other probes, whose penetration times scale quadratically with sample thickness, could diffuse much more rapidly through the specimen when physically thinned

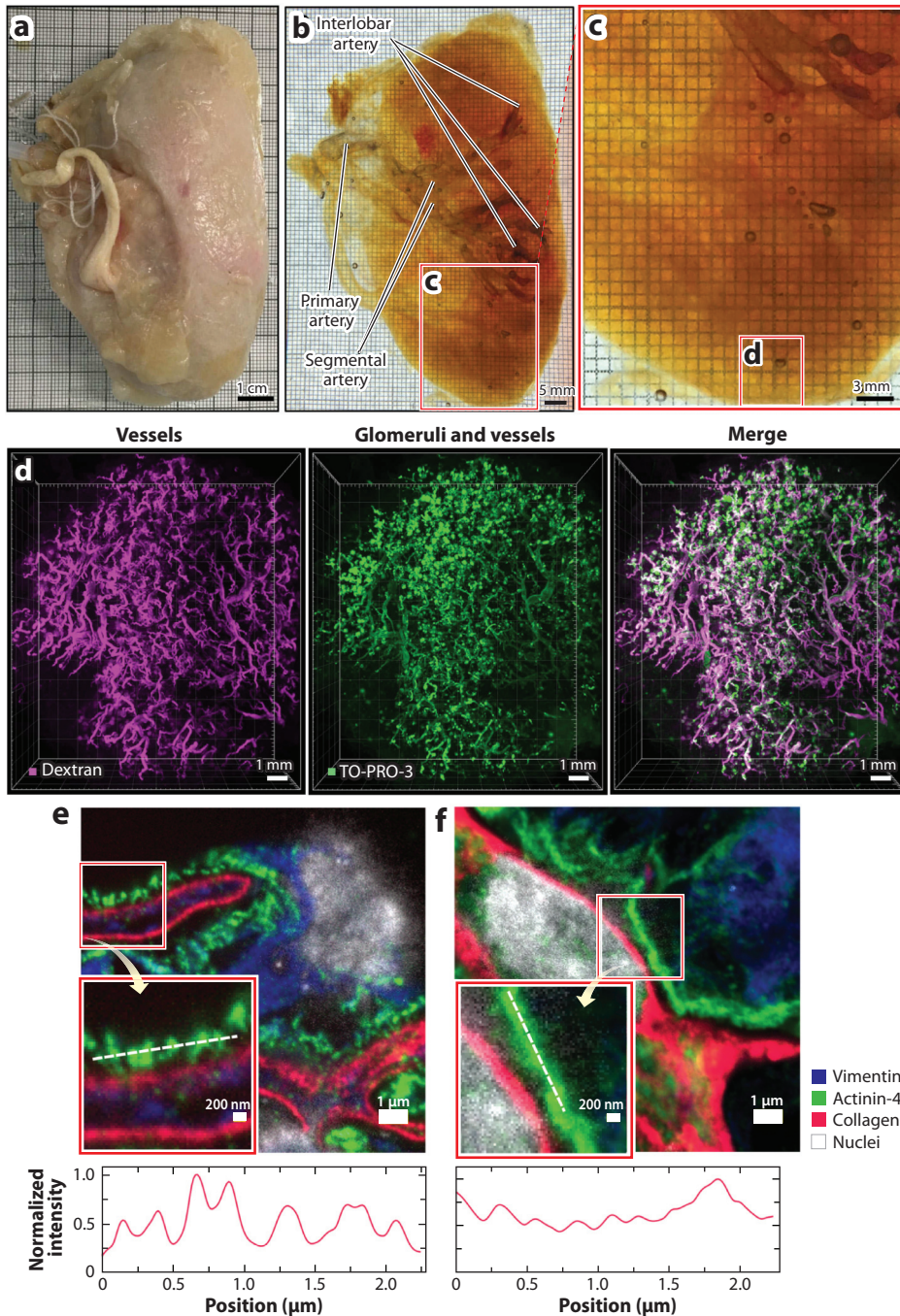


Figure 3

Clearing, expansion, and labeling of tissues. (a–d) Whole human kidney cleared via SHANEL, labeled with a dextran (magenta) and nuclear stain (green), and imaged by light-sheet microscopy to reveal blood vessels and glomeruli. (e,f) Human kidney sections imaged by confocal microscopy after hydrogel expansion and revealing differences between (e) a healthy patient and (f) a patient with minimal change disease. The specimens were antibody stained for vimentin (blue), actinin-4 (green), and collagen IV (red) and counterstained for nuclei (white). Insets show zoomed-in regions outlined by the red box. Line profiles for dotted lines in the inset show actinin-4 intensity normalized to maximum intensity. Panels a–d adapted from Reference 95 (CC BY 4.0). Panels e,f adapted with permission from Reference 101; copyright 2017 Springer Nature.

via stretching. However, the increased labeling speed is offset in part by the relatively long time of ~20 days required to create the tissue-gel specimen in the first place. Finally, stochastic electro-transport uses electric fields to enhance diffusion of antibodies and other charged species through tissue-gel specimens (105).

In a different approach for thick-tissue labeling and clearing, Susaki et al. (106) developed procedures called CUBIC-HV for one-step efficient and uniform staining of whole organs from model organisms by carefully tuning concentrations of detergent, antibody/probe, and additives such as quadrol, urea, and salt, while also controlling temperature. Indeed, the use of passive diffusion for chemical labeling can also be effective across whole human organs when implemented with procedures tailored for speed, such as SHANEL (**Figure 3d**) for labeling of whole human organs (95).

Small-molecule labels are powerful tools for staining pathology specimens and are also highly effective in 3D light-sheet microscopy. For some of our work, we have used noncovalent staining with common DNA-affinity dyes (e.g., DRAQ5, TO-PRO-3) to label nuclei, in conjunction with the general physiology stain, eosin, which has an affinity for basic structures including proteins (42, 45, 46). These combinations of stains enable a rapid and simple fluorescent analog of the traditional H&E pathology stain when implementing some image processing to convert the fluorescence images (acquired with grayscale cameras) to look like chromogenic (absorption-based) H&E histology (107–110) (**Figure 4a**). This moderately specific H&E-analog stain has even been used to train a deep learning-based algorithm to create computational immunostains based on training sets with specimens costained with the H&E analog and a highly specific antibody (82) (**Figure 4b**). This, in turn, enables image-translation-assisted segmentation in 3D (ITAS3D) for the 3D segmentation of diagnostically important tissue structures (e.g., prostate glands) without requiring tedious manual annotations or slow/expensive antibody staining (82).

We also recently developed a highly versatile, covalent labeling method called FLARE (fluorescent labeling of abundant reactive entities) that can covalently label amines and carbohydrates together with noncovalent labeling of DNA (94, 111–113). The amine and DNA stains again produce a fluorescent analog of H&E, while the concurrent carbohydrate stain provides a fluorescent analog of the traditional periodic acid Schiff histology stain widely used in pathology (107). The feature-rich tri-color stain (**Figure 4c–e**) has several useful attributes. First, the covalent stains, which are not removable by washing, are compatible with a wide range of protocols for clearing and expansion. Second, FLARE is compatible with other labeling procedures such as antibody labeling of specific proteins or FISH labeling of nucleic acids, and the specific dyes used for FLARE can be selected from a wide range of commercial dyes available across the entire visible spectrum. These small-molecule stains are generally bright and rapid owing to their small size and ability to label abundant general chemical targets on a sample.

In Situ Proteomics and Genomics

Standard fluorescence microscopes routinely image 3–5 channels, but there has been substantial interest in recent years in developing techniques that can image a larger number of channels in situ in order to concurrently study many proteins, messenger RNA (mRNA), DNA loci, or other molecules of interest. Many of these emerging techniques have primarily been applied to cells or 2D tissue sections, but the tools, broadly speaking, are highly promising for their potential applications in 3D pathology.

One approach to boost the number of channels for protein detection in optical imaging is to use multiple rounds of imaging, with antibody removal or fluorophore bleaching in between, such as with methods termed MxIF, t-CyCIF, CODEX, or IBEX (114–117). These techniques have been demonstrated for the imaging of tens of channels (**Figure 5**), typically on thin specimens,

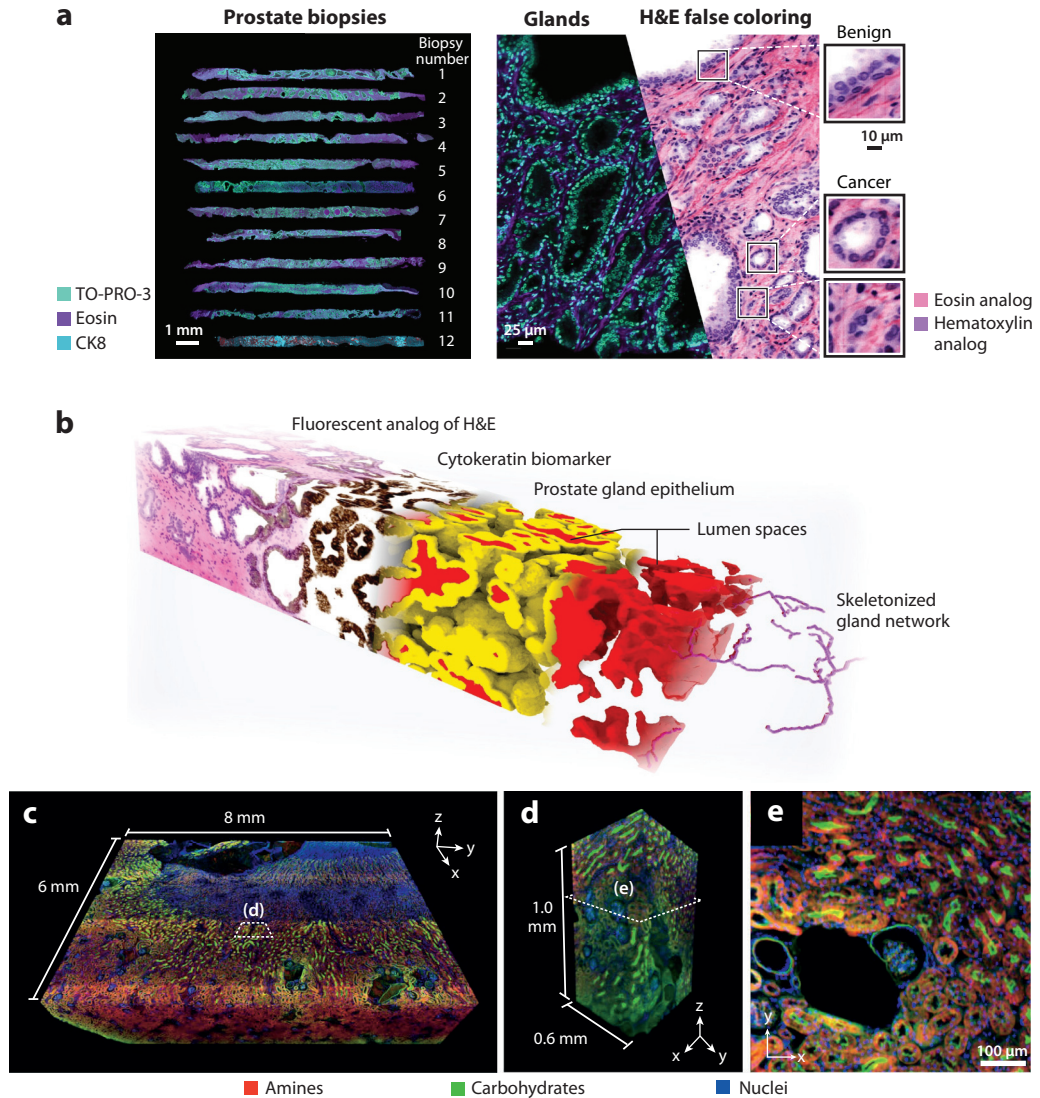


Figure 4

Fluorescent analogs of general physiology stains. (a) Cleared human prostate biopsies that have been stained with a fluorescent hematoxylin and eosin (H&E) analog and imaged by open-top light-sheet (OTLS) microscopy. Panel adapted from Reference 45 (CC BY 4.0). (b) A three-dimensional (3D) pathology data set of a prostate biopsy stained with a fluorescent analog of H&E (pink and purple region). Deep learning-based image translation was used to convert the H&E data set into a synthetic data set that looks like it has been immunolabeled to highlight a cytokeratin biomarker (brown) that is expressed by the epithelial cells in all prostate glands. In turn, this synthetically immunolabeled data set allows for accurate 3D segmentation of the prostate gland epithelium (yellow) and lumen spaces (red). Quantitative features derived from these segmented 3D structures are used to train a machine classifier to stratify between aggressive (recurrent) versus indolent (nonrecurrent) cancer (82). Panel adapted from Reference 82 (CC BY 4.0). (c–e) Cleared mouse kidney tissue that was labeled via FLARE [amines (red), carbohydrates (green), and nuclei (blue)] and imaged by OTLS. FLARE stains are fluorescent analogs of H&E and periodic acid Schiff stains. Panels c–e adapted from Reference 113.

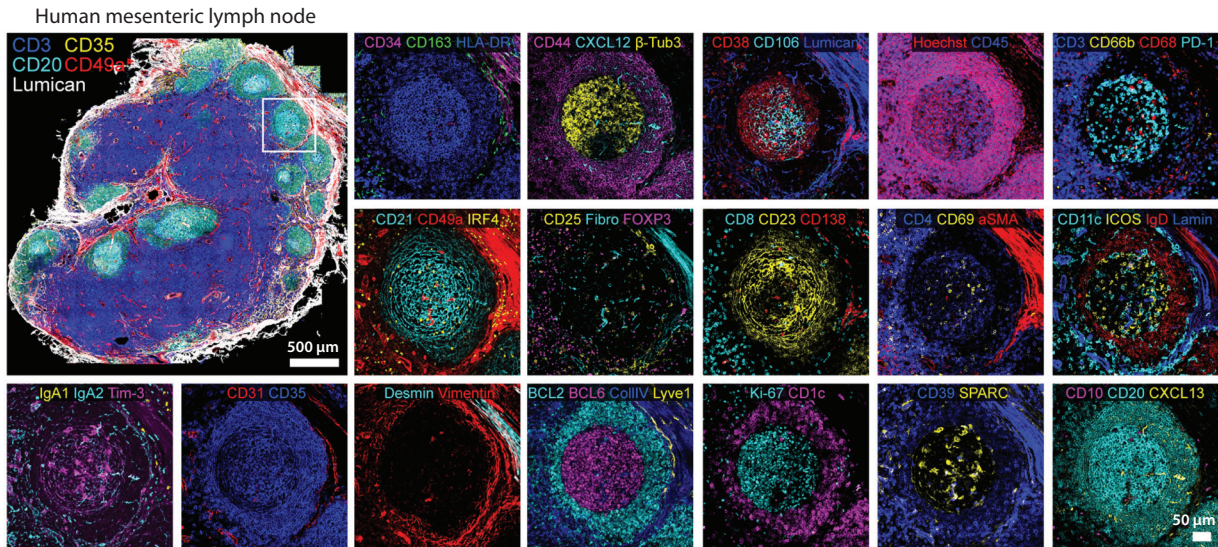


Figure 5

In situ proteomics in human tissues. Human lymph node studied by IBEX using iterative staining and confocal microscopy at 66 channels. Names in the figure indicate 66 different antibodies that were used to target key structures in the human mesenteric lymph node. Panels adapted from Reference 117.

although, for instance, Murray et al. (103) demonstrated the use of SWITCH to perform up to ~20 rounds of sequential labeling and imaging in hydrogel-stabilized mouse brain tissues.

Rather than study protein abundance through highly multiplexed antibody labeling, some approaches have sought to study mRNA because mRNA abundance can be a good proxy for protein expression (118) and mRNA can be readily targeted by FISH for nearly any gene. For example, MERFISH and seqFISH use encoded multi-round FISH techniques to detect hundreds to thousands of mRNA targets (119, 120), FISSEQ and STARmap utilize in situ sequencing for mRNA detection with workflows based on next-generation sequencing pipelines (121, 122), and spatial transcriptomics and DBiT-seq use spatial barcoding by a substrate or microfluidics device, respectively, to tag mRNA from specific regions of a specimen with barcodes that can be decoded during sequencing (123, 124). These and other methods for spatially resolved detection of mRNA are rapidly evolving and hold great promise for the study of pathology samples at single-cell resolution with high mRNA detection efficiency and genome-wide coverage. Several commercial efforts have gained traction in this area and have been used in studies of human pathology specimens, albeit typically in two dimensions. For example, a commercial implementation of spatial transcriptomics from Visium has been used to study breast cancer tissues (**Figure 6**), revealing details of the tumor microenvironment such as metabolic reprogramming and obtaining new findings that may be helpful for diagnosis or treatment (125). In addition, the GeoMx platform from NanoString, which uses spatially photocleavable DNA barcodes to target panels of mRNA (or proteins) (126), is used for targeted analysis of small regions of tissue, including for the study of lung injury in humans resulting from COVID-19 infection (127).

FUTURE DIRECTIONS

A wealth of opportunities for nondestructive 3D pathology can be applied in diverse areas that can impact patient care, from translational research and preclinical drug development to clinical

Guest (guest)

IP: 13.58.121.251

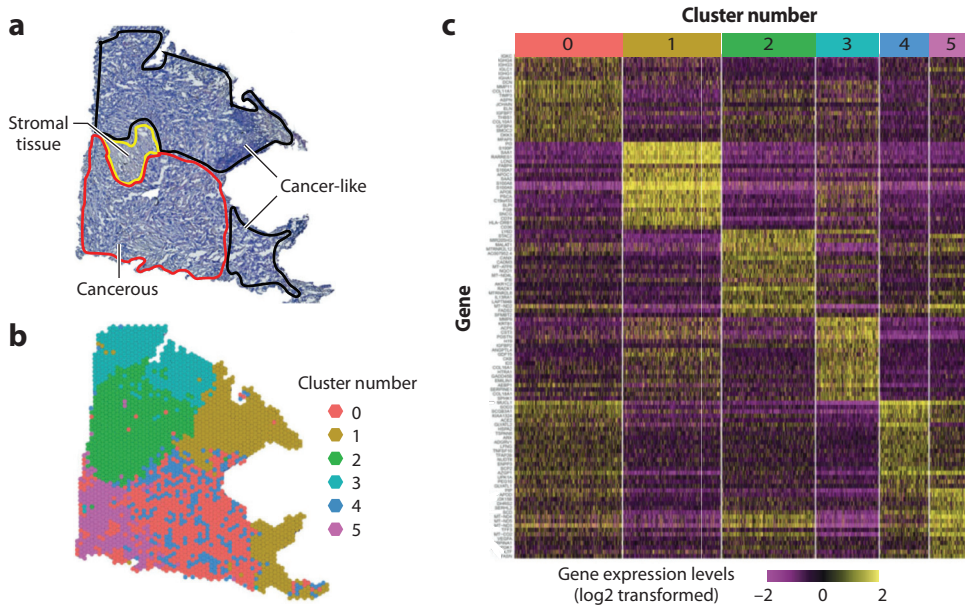


Figure 6

In situ transcriptomics in human tissues. (a) Breast cancer tumor tissue section stained with hematoxylin and eosin (H&E). (b) Spatial transcriptomics data corresponding to panel a with transcriptomic-based clustering indicated by color of dot. (c) Heat map of highly differentially expressed genes for clusters in panel b. Figure adapted from Reference 125 (CC BY 4.0).

assays. Each of these scenarios offers multiple ways in which complementary technologies and methods may be coupled with 3D pathology to provide novel capabilities, some of which are outlined below.

For translational investigations, 3D tissue models, such as spheroids and organoids, are increasingly valued over traditional 2D tissue cultures (i.e., cell monolayers in a dish), as shown in **Figure 7**. Such constructs recapitulate the complex and heterogeneous microenvironment of tissues with high fidelity and thus lead to insights that translate more readily to human biology.

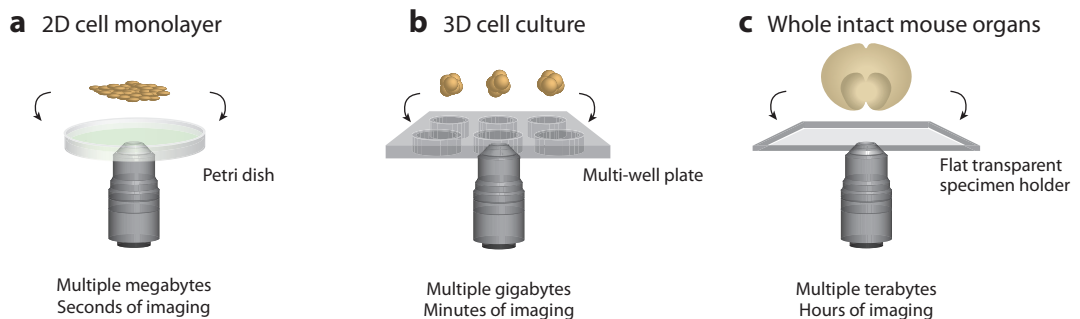


Figure 7

Microscopy from cells and organoids to organisms. There are clear advantages in terms of biological realism and insights when imaging whole organisms or 3D cultures versus traditional cell monolayers on petri dishes. However, there are exponentially greater challenges in terms of imaging speed/throughput and data set sizes. With 3D pathology methods, the computational hurdles represent the next frontier for many biological and clinical applications. Abbreviations: 2D, two-dimensional; 3D, three-dimensional.

Guest (guest)

There is an obvious need and value for high-throughput volumetric imaging of such tissue constructs, including *in vitro* imaging of dynamic processes over time. As living cells and tissues, even at the scale of a few hundreds of microns, contain refractive heterogeneities that lead to light scattering and aberrations, there is a technical challenge for volumetric microscopy approaches to mitigate these effects for deep imaging with high contrast and resolution. Examples include adaptive optics techniques to dynamically compensate for tissue-induced aberrations (128–131) and multiview imaging approaches that can provide a larger volumetric field of view by viewing the specimen from different angles and/or directions (33, 132–134).

For translational investigations and preclinical drug development, the use of animal models, and especially rodent models, will continue to be an important and necessary step toward gaining improved insights and for hypothesis testing in preparation for human studies. Here, a major challenge for 3D pathology is the size of the tissues that must often be interrogated, which can approximate the size of clinical lesions (i.e., millimeters to centimeters in extent). This introduces challenges for not only tissue labeling and clearing but also imaging times, data storage, and big-data analysis. Tissue labeling can be particularly challenging. While animal models can often be engineered to express fluorescent proteins, clever approaches are being devised (as mentioned previously) to facilitate rapid exogenous labeling with small and large molecules (e.g., antibodies) as well as rapid optical clearing of entire organs (e.g., mouse brains) and organisms (e.g., whole mice). Finally, with the popularity of approaches for massively multiplexed DNA and RNA *in situ* hybridization and whole-genome/-transcriptome sequencing of 2D histology sections, there is a push toward extending these spatial biology and spatial omics techniques into 3D tissues. This will necessitate additional advances in automated fluidic buffer exchanges for cyclic barcoding and labeling rounds and other innovative approaches for imaging highly multiplexed information from 3D tissue volumes labeled with diverse molecular probes.

In a previous section, we outlined some of the challenges and solutions being devised to handle the acquisition and immediate postprocessing of large 3D pathology data sets. For example, multiresolution imaging workflows will likely be essential for most applications of 3D pathology in the near future, other than large-scale efforts in neuroscience and other big-science endeavors supported by large philanthropy or governmental mandates. For downstream image analysis, however, many more challenges exist. Although a discussion on machine learning and image analysis methods is beyond the scope of this article, a major challenge for the field of machine learning will be to generate ground-truth annotations for 3D segmentation and classification (135, 136). Recent efforts in weakly supervised learning and annotation-free segmentation are attempting to overcome some of these barriers (82, 137–140). Another challenge is the memory constraints of current graphics processing units (GPUs), which limit the ability to process high-resolution 3D pathology data sets over sufficiently large chunk volumes to capture the necessary spatial context for diagnostic determinations (141). Even if chunk sizes can be accommodated by GPUs, training and inference times can still be prohibitive without parallelization across large banks of GPU arrays. An interim solution may be to analyze 3D pathology data sets as stacks of individual 2D images, or with 2.5D methods that incorporate the information from a few adjacent 2D levels to improve the analysis of each 2D cross section within a volumetric stack (82, 142, 143).

For preclinical drug development, the value proposition for 3D pathology includes the ability to identify mechanisms of action for lead candidates and to identify toxicities at earlier stages. Both of these goals can translate into significant cost and time savings for researchers and pharma companies. It is likely that drug developers will play a significant role as early adopters of 3D pathology, helping to refine these methods and paving the way for clinical adoption in the future.

Clinical applications of 3D pathology can be largely grouped into (a) early and accurate diagnosis, (b) improved prognostication for clinical decision support, and (c) predictive assays to identify

ideal patient candidates for specific treatments such as chemotherapy and immunotherapies. As detailed in a recent perspective article (144), 3D pathology has the potential to complement traditional 2D histology by offering orders-of-magnitude more tissue coverage with volumetric insights. This will enable a more accurate quantification of complex tissue structures, such as glandular networks that are disrupted in a predictable way as a function of disease progression and aggressiveness. It will also enable improved quantification of complex cell distributions that are highly heterogeneous, such as the tumor-immune microenvironment that plays a critical role in patient prognosis and response to various drug therapies (and especially immunotherapies). Finally, there are many rare events that are difficult to spot on 2D histology sections due to the minimal amount of tissue that is sampled by such techniques, but which can be more readily identified and quantified through 3D pathology of large tissue volumes. Examples of such rare events that hold prognostic importance include tumor cells showing signs of premetastatic behavior (e.g., lymphovascular invasion and perineural invasion) and minimal-residual disease after radiation or chemotherapy.

To provide equitable and accurate clinical decision support, computational pathology (i.e., pathomics) should ideally be combined with other modalities such as radiomics and genomics, as well as with clinical data in electronic health records. The advantage of 3D pathology is that it can enhance other omics technologies within the clinic. For example, nondestructive imaging will allow larger amounts of tissue to be available for downstream molecular analyses. In addition, scanning large tissue volumes versus thin tissue sections will enable improved coregistration with radiology images for combined pathomic and radiomic analyses.

SUMMARY

In this review, we have outlined the potential biomedical impact and technical challenges of non-destructive 3D pathology. In terms of the technical strategies behind various implementations of 3D pathology, **Figure 8** provides a list of some of the most common steps that we have mentioned

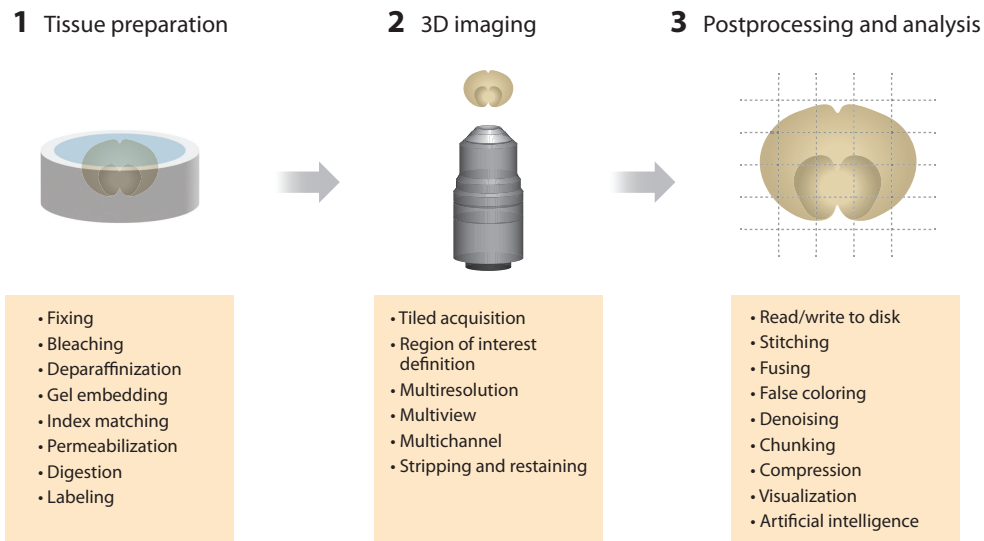


Figure 8

Examples of key considerations and steps in three-dimensional (3D) pathology. Various applications of 3D pathology will each have unique technical requirements and timescales for tissue preparation, high-throughput 3D microscopy, and data handling/analysis. A few examples of technical steps are listed.

for tissue preparation, 3D imaging, and data processing/analysis. Many future innovations will focus on improving the throughput of these various steps, ideally shifting the timescales from days and hours to minutes. As discussed in the previous section, exciting new applications of 3D pathology, ranging from translational research and preclinical drug development to clinical assays, will continue to emerge with the hopes that many of them will be rigorously validated and incorporated into standard preclinical and clinical workflows.

DISCLOSURE STATEMENT

J.T.C.L. is a cofounder, equity holder, and board member of Alpenglow Biosciences, Inc. A.K.G. is a cofounder and equity holder of Alpenglow Biosciences, Inc. The other authors are not aware of any affiliations, memberships, funding, or financial holdings that might be perceived as affecting the objectivity of this review.

ACKNOWLEDGMENTS

The authors acknowledge funding support from the Department of Defense (DoD) Prostate Cancer Research Program (PCRP) through W81WH-18-10358 (J.T.C.L.), the National Cancer Institute (NCI) through R01CA268207 (J.T.C.L.) and R00CA240681 (A.K.G.), the National Institute of Biomedical Imaging and Bioengineering (NIBIB) through R01EB031002 (J.T.C.L.), the Prostate Cancer United Kingdom (PCUK) charity (J.T.C.L.), the National Science Foundation (NSF) 1934292 HDR: I-DIRSE-FW (J.T.C.L.), the National Institute of Mental Health through R01MH115767 (J.C.V.), and the Washington Research Foundation Postdoctoral Fellowship (C.P.).

LITERATURE CITED

1. Abeytunge S, Li Y, Larson B, Peterson G, Seltzer E, et al. 2013. Confocal microscopy with strip mosaicing for rapid imaging over large areas of excised tissue. *J. Biomed. Opt.* 18:61227
2. Helmchen F, Denk W. 2005. Deep tissue two-photon microscopy. *Nat. Methods* 2:932–40
3. Tao YK, Shen D, Sheikine Y, Ahsen OO, Wang HH, et al. 2014. Assessment of breast pathologies using nonlinear microscopy. *PNAS* 111:15304–9
4. Tu H, Liu Y, Turchinovich D, Marjanovic M, Lyngsø J, et al. 2016. Stain-free histopathology by programmable supercontinuum pulses. *Nat. Photon.* 10:534–40
5. Yoshitake T, Giacomelli MG, Cahill LC, Schmolze DB, Vardeh H, et al. 2016. Direct comparison between confocal and multiphoton microscopy for rapid histopathological evaluation of unfixed human breast tissue. *J. Biomed. Opt.* 21:126021
6. Mayerich D, Abbott L, McCormick B. 2008. Knife-edge scanning microscopy for imaging and reconstruction of three-dimensional anatomical structures of the mouse brain. *J. Microsc.* 231:134–43
7. Humphrey PA. 1993. Complete histologic serial sectioning of a prostate gland with adenocarcinoma. *Am. J. Surg. Pathol.* 17:468–72
8. Li A, Gong H, Zhang B, Wang Q, Yan C, et al. 2010. Micro-optical sectioning tomography to obtain a high-resolution atlas of the mouse brain. *Science* 330:1404–8
9. Shimozawa T, Yamagata K, Kondo T, Hayashi S, Shitamukai A, et al. 2013. Improving spinning disk confocal microscopy by preventing pinhole cross-talk for intravital imaging. *PNAS* 110:3399–404
10. Nakano A. 2002. Spinning-disk confocal microscopy—a cutting-edge tool for imaging of membrane traffic. *Cell Struct. Funct.* 27:349–55
11. Bewersdorf J, Pick R, Hell SW. 1998. Multifocal multiphoton microscopy. *Opt. Lett.* 23:655–57
12. Bahlmann K, So PT, Kirber M, Reich R, Kosicki B, et al. 2007. Multifocal multiphoton microscopy (MMM) at a frame rate beyond 600 Hz. *Opt. Express* 15:10991–98
13. Oron D, Tal E, Silberberg Y. 2005. Scanningless depth-resolved microscopy. *Opt. Express* 13:1468–76

Downloaded from www.annualreviews.org.

Guest (guest)

14. Liu JTC, Mandella MJ, Loewke NO, Haeberle H, Ra H, et al. 2010. Micromirror-scanned dual-axis confocal microscope utilizing a gradient-index relay lens for image guidance during brain surgery. *J. Biomed. Opt.* 15:026029
15. Bishop KW, Maitland KC, Rajadhyaksha M, Liu JTC. 2022. In vivo microscopy as an adjunctive tool to guide detection, diagnosis, and treatment. *J. Biomed. Opt.* 27:040601
16. Flusberg BA, Jung JC, Cocker ED, Anderson EP, Schnitzer MJ. 2005. In vivo brain imaging using a portable 3.9 gram two-photon fluorescence microendoscope. *Opt. Lett.* 30:2272–74
17. Piyawattanametha W, Cocker ED, Burns LD, Barretto RP, Jung JC, et al. 2009. In vivo brain imaging using a portable 2.9 g two-photon microscope based on a microelectromechanical systems scanning mirror. *Opt. Lett.* 34:2309–11
18. Yin C, Glaser AK, Leigh SY, Chen Y, Wei L, et al. 2016. Miniature in vivo MEMS-based line-scanned dual-axis confocal microscope for point-of-care pathology. *Biomed. Opt. Express* 7:251–63
19. Sanai N, Snyder LA, Honea NJ, Coons SW, Eschbacher JM, et al. 2011. Intraoperative confocal microscopy in the visualization of 5-aminolevulinic acid fluorescence in low-grade gliomas. *J. Neurosurg.* 115:740–48
20. Moen E, Bannon D, Kudo T, Graf W, Covert M, Van Valen D. 2019. Deep learning for cellular image analysis. *Nat. Methods* 16:1233–46
21. Belthangady C, Royer LA. 2019. Applications, promises, and pitfalls of deep learning for fluorescence image reconstruction. *Nat. Methods* 16:1215–25
22. Bera K, Schalper KA, Rimm DL, Velcheti V, Madabhushi A. 2019. Artificial intelligence in digital pathology—new tools for diagnosis and precision oncology. *Nat. Rev. Clin. Oncol.* 16:703–15
23. Niazi MKK, Parwani AV, Gurcan MN. 2019. Digital pathology and artificial intelligence. *Lancet Oncol.* 20:e253–61
24. Wang Z, Chen J, Hoi SC. 2020. Deep learning for image super-resolution: a survey. *IEEE Trans. Pattern Anal. Mach. Intell.* 43:3365–87
25. Dong C, Loy CC, He K, Tang X. 2014. Learning a deep convolutional network for image super-resolution. *Comp. Vis. ECCV* 2014:184–99
26. Wang H, Rivenson Y, Jin Y, Wei Z, Gao R, et al. 2019. Deep learning enables cross-modality super-resolution in fluorescence microscopy. *Nat. Methods* 16:103–10
27. Weigert M, Schmidt U, Boothe T, Müller A, Dibrov A, et al. 2018. Content-aware image restoration: pushing the limits of fluorescence microscopy. *Nat. Methods* 15:1090–97
28. Liu Z, Keller PJ. 2016. Emerging imaging and genomic tools for developmental systems biology. *Dev. Cell* 36:597–610
29. Huisken J, Stainier DYS. 2009. Selective plane illumination microscopy techniques in developmental biology. *Development* 136:1963–75
30. Siedentopf H, Zsigmondy R. 1902. Über Sichtbarmachung und Größenbestimmung ultramikroskopischer Teilchen, mit besonderer Anwendung auf Goldrubingläser. *Ann. Phys.* 315:1–39
31. Siedentopf H. 1903. On the rendering visible of ultra-microscopic particles and of ultra-microscopic bacteria. *J. R. Microsc. Soc.* 23:573–78
32. Voie AH, Burns DH, Spelman FA. 1993. Orthogonal-plane fluorescence optical sectioning: three-dimensional imaging of macroscopic biological specimens. *J. Microsc.* 170:229–36
33. Huisken J, Swoger J, Del Bene F, Wittbrodt J, Stelzer EHK. 2004. Optical sectioning deep inside live embryos by selective plane illumination microscopy. *Science* 305:1007–9
34. Keller PJ, Schmidt AD, Wittbrodt J, Stelzer EHK. 2008. Reconstruction of zebrafish early embryonic development by scanned light sheet microscopy. *Science* 322:1065–69
35. Mickoleit M, Schmid B, Weber M, Fahrbach FO, Hombach S, et al. 2014. High-resolution reconstruction of the beating zebrafish heart. *Nat. Methods* 11:919–22
36. Keller PJ, Ahrens MB. 2015. Visualizing whole-brain activity and development at the single-cell level using light-sheet microscopy. *Neuron* 85:462–83
37. Power RM, Huisken J. 2017. A guide to light-sheet fluorescence microscopy for multiscale imaging. *Nat. Methods* 14:360–73
38. Kumar A, Wu Y, Christensen R, Chandris P, Gandler W, et al. 2014. Dual-view plane illumination microscopy for rapid and spatially isotropic imaging. *Nat. Protoc.* 9:2555–73

39. Strnad P, Gunther S, Reichmann J, Krzic U, Balazs B, et al. 2015. Inverted light-sheet microscope for imaging mouse pre-implantation development. *Nat. Methods* 13:139–42
40. McGorty R, Liu H, Kamiyama D, Dong Z, Guo S, Huang B. 2015. Open-top selective plane illumination microscope for conventionally mounted specimens. *Opt. Express* 23:16142–53
41. McGorty R, Xie D, Huang B. 2017. High-NA open-top selective-plane illumination microscope for biological imaging. *Opt. Express* 25:17798–810
42. Glaser AK, Reder NP, Chen Y, McCarty EF, Yin C, et al. 2017. Light-sheet microscopy for slide-free non-destructive pathology of large clinical specimens. *Nat. Biomed. Eng.* 1:0084
43. Barner LA, Glaser AK, True LD, Reder NP, Liu JTC. 2019. Solid immersion meniscus lens (SIMlens) for open-top light-sheet microscopy. *Opt. Lett.* 44:4451–54
44. Barner LA, Glaser AK, Huang H, True LD, Liu JTC. 2020. Multi-resolution open-top light-sheet microscopy to enable efficient 3D pathology workflows. *Biomed. Opt. Express* 11:6605–19
45. Glaser AK, Reder NP, Chen Y, Yin C, Wei L, et al. 2019. Multi-immersion open-top light-sheet microscope for high-throughput imaging of cleared tissues. *Nat. Commun.* 10:2781
46. Glaser AK, Bishop KW, Barner LA, Susaki EA, Kubota SI, et al. 2022. A hybrid open-top light-sheet microscope for versatile multi-scale imaging of cleared tissues. *Nat. Methods* 19:613–19
47. Botcherby EJ, Juškaitis R, Booth MJ, Wilson T. 2008. An optical technique for remote focusing in microscopy. *Opt. Commun.* 281:880–87
48. Dunsby C. 2008. Optically sectioned imaging by oblique plane microscopy. *Opt. Express* 16:20306–16
49. Voleti V, Patel KB, Li W, Perez Campos C, Bharadwaj S, et al. 2019. Real-time volumetric microscopy of in vivo dynamics and large-scale samples with SCAPE 2.0. *Nat. Methods* 16:1054–62
50. Bouchard MB, Voleti V, Mendes CS, Laceyfield C, Grueber WB, et al. 2015. Swept confocally-aligned planar excitation (SCAPE) microscopy for high-speed volumetric imaging of behaving organisms. *Nat. Photon.* 9:113–19
51. Yang B, Chen X, Wang Y, Feng S, Pessino V, et al. 2019. Epi-illumination SPIM for volumetric imaging with high spatial-temporal resolution. *Nat. Methods* 16:501–4
52. Millett-Sikking A, York A. 2019. *High NA single-objective light-sheet: work in progress*. Zenodo, version 0.0.2. <https://doi.org/10.5281/zenodo.3244420>
53. Kumar M, Kishore S, Nasenbeny J, McLean DL, Kozorovitskiy Y. 2018. Integrated one- and two-photon scanned oblique plane illumination (SOPi) microscopy for rapid volumetric imaging. *Opt. Express* 26:13027–41
54. Hoffmann M, Judkewitz B. 2019. Diffractive oblique plane microscopy. *Optica* 6:5
55. Sapoznik E, Chang B-J, Huh J, Ju RJ, Azarova EV, et al. 2020. A versatile oblique plane microscope for large-scale and high-resolution imaging of subcellular dynamics. *eLife* 9:e57681
56. Yang B, Lange M, Millett-Sikking A, Solak AC, Kumar SV, et al. 2021. High-resolution, large imaging volume, and multi-view single objective light-sheet microscopy. bioRxiv 309229. <https://doi.org/10.1101/2020.09.22.309229>
57. Li T, Ota S, Kim J, Wong ZJ, Wang Y, et al. 2014. Axial plane optical microscopy. *Sci. Rep.* 4:7253
58. Kim J, Wojcik M, Wang Y, Moon S, Zin EA, et al. 2019. Oblique-plane single-molecule localization microscopy for tissues and small intact animals. *Nat. Methods* 16:853–57
59. Migliori B, Datta MS, Dupre C, Apak MC, Asano S, et al. 2018. Light sheet theta microscopy for rapid high-resolution imaging of large biological samples. *BMC Biol.* 16:57
60. Keller PJ, Schmidt AD, Santella A, Khairy K, Bao Z, et al. 2010. Fast, high-contrast imaging of animal development with scanned light sheet-based structured-illumination microscopy. *Nat. Methods* 7:637–42
61. Hoyer P, de Medeiros G, Balázs B, Norlin N, Besir C, et al. 2016. Breaking the diffraction limit of light-sheet fluorescence microscopy by RESOLFT. *PNAS* 113:3442–46
62. Friedrich M, Gan Q, Ermolayev V, Harms GS. 2011. STED-SPIM: Stimulated emission depletion improves sheet illumination microscopy resolution. *Biophys. J.* 100:L43–45
63. Zhao F, Zhu L, Fang C, Yu T, Zhu D, Fei P. 2020. Deep-learning super-resolution light-sheet add-on microscopy (Deep-SLAM) for easy isotropic volumetric imaging of large biological specimens. *Biomed. Opt. Express* 11:7273–85
64. Dean KM, Roudot P, Welf ES, Danuser G, Fiolka R. 2015. Deconvolution-free subcellular imaging with axially swept light sheet microscopy. *Biophys. J.* 108:2807–15

65. Fu Q, Martin BL, Matus DQ, Gao L. 2016. Imaging multicellular specimens with real-time optimized tiling light-sheet selective plane illumination microscopy. *Nat. Commun.* 7:11088
66. Rohrbach A, Fahrbach FO, Alessandri K, Nassoy P, Gurchenkov V. 2013. Self-reconstructing sectioned Bessel beams offer submicron optical sectioning for large fields of view in light-sheet microscopy. *Opt. Express* 21:11425–40
67. Fahrbach FO, Simon P, Rohrbach A. 2010. Microscopy with self-reconstructing beams. *Nat. Photon.* 4:780–85
68. Planchon TA, Gao L, Milkie DE, Davidson MW, Galbraith JA, et al. 2011. Rapid three-dimensional isotropic imaging of living cells using Bessel beam plane illumination. *Nat. Methods* 8:417–23
69. Vettenburg T, Dalgarno HIC, Nytk J, Coll-Lladó C, Ferrier DEK, et al. 2014. Light-sheet microscopy using an Airy beam. *Nat. Methods* 11:541–44
70. Remacha E, Friedrich L, Vermot J, Fahrbach FO. 2020. How to define and optimize axial resolution in light-sheet microscopy: a simulation-based approach. *Biomed. Opt. Express* 11:8–26
71. Shi Y, Daugird TA, Legant WR. 2022. A quantitative analysis of various patterns applied in lattice light sheet microscopy. *Nat. Commun.* 13:4607
72. Chang BJ, Dean KM, Fiolka R. 2020. Systematic and quantitative comparison of lattice and Gaussian light-sheets. *Opt. Express* 28:27052–77
73. Reynaud EG, Peychl J, Huisken J, Tömancák P. 2014. Guide to light-sheet microscopy for adventurous biologists. *Nat. Methods* 12:30–34
74. Battistella E, Quintana JF, McConnell G. 2022. Application of light-sheet mesoscopy to image host-pathogen interactions in intact organs. *Front. Cell. Infect. Microbiol.* 12:903957
75. Amat F, Hockendorf B, Wan Y, Lemon WC, McDole K, Keller PJ. 2015. Efficient processing and analysis of large-scale light-sheet microscopy data. *Nat. Protoc.* 10:1679–96
76. Gibbs HC, Mota SM, Hart NA, Min SW, Vernino AO, et al. 2021. Navigating the light-sheet image analysis software landscape: concepts for driving cohesion from data acquisition to analysis. *Front. Cell Dev. Biol.* 9:739079
77. Andreev A, Koo DES. 2020. Practical guide to storage of large amounts of microscopy data. *Microsc. Today* 28:42–45
78. Balazs B, Deschamps J, Albert M, Ries J, Hufnagel L. 2017. A real-time compression library for microscopy images. bioRxiv 164624. <https://doi.org/10.1101/164624>
79. Beati I, Andreica E, Majer P. 2020. ImarisWriter: open source software for storage of large images in blockwise multi-resolution format. arXiv 10311. <https://arxiv.org/abs/2008.10311>
80. Hörl D, Rusak FR, Preusser F, Tillberg P, Randel N, et al. 2019. BigStitcher: reconstructing high-resolution image datasets of cleared and expanded samples. *Nat. Methods* 16:870–74
81. Bria A, Iannello G. 2012. TeraStitcher—a tool for fast automatic 3D-stitching of teravoxel-sized microscopy images. *BMC Bioinform.* 13:316
82. Xie W, Reder NP, Koyuncu C, Leo P, Hawley S, et al. 2022. Prostate cancer risk stratification via nondestructive 3D pathology with deep learning–assisted gland analysis. *Cancer Res.* 82:334–45
83. Richardson DS, Lichtman JW. 2015. Clarifying tissue clearing. *Cell* 162:246–57
84. Tainaka K, Kuno A, Kubota SI, Murakami T, Ueda HR. 2016. Chemical principles in tissue clearing and staining protocols for whole-body cell profiling. *Annu. Rev. Cell Dev. Biol.* 32:713–41
85. Almagro J, Messal HA, Zaw Thin M, van Rheenen J, Behrens A. 2021. Tissue clearing to examine tumour complexity in three dimensions. *Nat. Rev. Cancer* 21:718–30
86. Molbay M, Kolabas ZI, Todorov MI, Ohn TL, Ertürk A. 2021. A guidebook for DISCO tissue clearing. *Mol. Syst. Biol.* 17:e9807
87. Choi SW, Guan W, Chung K. 2021. Basic principles of hydrogel-based tissue transformation technologies and their applications. *Cell* 184:4115–36
88. Richardson DS, Guan W, Matsumoto K, Pan C, Chung K, et al. 2021. Tissue clearing. *Nat. Rev. Methods Primers* 1:84
89. Ke M-T, Fujimoto S, Imai T. 2013. SeeDB: a simple and morphology-preserving optical clearing agent for neuronal circuit reconstruction. *Nat. Neurosci.* 16:1154–61
90. Hou B, Zhang D, Zhao S, Wei M, Yang Z, et al. 2015. Scalable and DiI-compatible optical clearance of the mammalian brain. *Front. Neuroanat.* 9:19

91. Klingberg A, Hasenberg A, Ludwig-Portugall I, Medyukhina A, Männ L, et al. 2017. Fully automated evaluation of total glomerular number and capillary tuft size in nephritic kidneys using lightsheet microscopy. *J. Am. Soc. Nephrol.* 28:452–59
92. Nojima S, Susaki EA, Yoshida K, Takemoto H, Tsujimura N, et al. 2017. CUBIC pathology: three-dimensional imaging for pathological diagnosis. *Sci. Rep.* 7:9269
93. Tanaka N, Kanatani S, Tomer R, Sahlgren C, Kronqvist P, et al. 2017. Whole-tissue biopsy phenotyping of three-dimensional tumours reveals patterns of cancer heterogeneity. *Nat. Biomed. Eng.* 1:796–806
94. Barner LA, Glaser AK, Mao C, Susaki EA, Vaughan JC, et al. 2022. Multiresolution nondestructive 3D pathology of whole lymph nodes for breast cancer staging. *J. Biomed. Opt.* 27:036501–13
95. Zhao S, Todorov MI, Cai R, Al-Maskari R, Steinke H, et al. 2020. Cellular and molecular probing of intact human organs. *Cell* 180:796–812.e19
96. Chen F, Tillberg PW, Boyden ES. 2015. Expansion microscopy. *Science* 347:543–48
97. Chozinski TJ, Halpern AR, Okawa H, Kim H-J, Tremel GJ, et al. 2016. Expansion microscopy with conventional antibodies and fluorescent proteins. *Nat. Methods* 13:485–88
98. Ku T, Swaney J, Park J-Y, Albanese A, Murray E, et al. 2016. Multiplexed and scalable super-resolution imaging of three-dimensional protein localization in size-adjustable tissues. *Nat. Biotechnol.* 34:973–81
99. Tillberg PW, Chen F. 2019. Expansion microscopy: scalable and convenient super-resolution microscopy. *Annu. Rev. Cell Dev. Biol.* 35:683–701
100. Wassie AT, Zhao Y, Boyden ES. 2019. Expansion microscopy: principles and uses in biological research. *Nat. Methods* 16:33–41
101. Zhao Y, Bucur O, Irshad H, Chen F, Weins A, et al. 2017. Nanoscale imaging of clinical specimens using pathology-optimized expansion microscopy. *Nat. Biotechnol.* 35:757–64
102. Valdes PA, Yu C-CJ, Aronson J, Zhao Y, Bernstock JD, et al. 2021. Decrowding expansion pathology: unmasking previously invisible nanostructures and cells in intact human brain pathology specimens. bioRxiv 471271. <https://doi.org/10.1101/2021.12.05.471271>
103. Murray E, Cho HH, Goodwin D, Ku T, Swaney J, et al. 2015. Simple, scalable proteomic imaging for high-dimensional profiling of intact systems. *Cell* 163:1500–14
104. Ku T, Guan W, Evans NB, Sohn CH, Albanese A, et al. 2020. Elasticizing tissues for reversible shape transformation and accelerated molecular labeling. *Nat. Methods* 17:609–13
105. Kim S-Y, Cho JH, Murray E, Bakh N, Choi H, et al. 2015. Stochastic electrotransport selectively enhances the transport of highly electromobile molecules. *PNAS* 112:E6274–83
106. Susaki EA, Shimizu C, Kuno A, Tainaka K, Li X, et al. 2020. Versatile whole-organ/body staining and imaging based on electrolyte-gel properties of biological tissues. *Nat. Commun.* 11:1982
107. Bancroft JD, Gamble M, eds. 2013. *Theory and Practice of Histological Techniques*. Edinburgh, UK: Churchill Livingstone
108. Giacomelli MG, Husvogt L, Vardeh H, Faulkner-Jones BE, Hornegger J, et al. 2016. Virtual hematoxylin and eosin transillumination microscopy using epi-fluorescence imaging. *PLOS ONE* 11:e0159337
109. Elfer KN, Sholl AB, Wang M, Tulman DB, Mandava SH, et al. 2016. DRAQ5 and eosin (‘D&E’) as an analog to hematoxylin and eosin for rapid fluorescence histology of fresh tissues. *PLOS ONE* 11:e0165530
110. Serafin R, Xie W, Glaser AK, Liu JTC. 2020. FalseColor-Python: a rapid intensity-leveling and digital-staining package for fluorescence-based slide-free digital pathology. *PLOS ONE* 15:e0233198
111. Chen Y, Xie W, Glaser AK, Reder NP, Mao C, et al. 2019. Rapid pathology of lumpectomy margins with open-top light-sheet (OTLS) microscopy. *Biomed. Opt. Express* 10:1257–72
112. Mao C, Lee MY, Jhan J-R, Halpern AR, Woodworth MA, et al. 2020. Feature-rich covalent stains for super-resolution and cleared tissue fluorescence microscopy. *Sci. Adv.* 6:eaba4542
113. Lee MY, Mao C, Glaser AK, Woodworth MA, Halpern AR, et al. 2022. Fluorescent labeling of abundant reactive entities (FLARE) for cleared-tissue and super-resolution microscopy. *Nat. Protoc.* 17:819–46
114. Gerdes MJ, Sevinsky CJ, Sood A, Adak S, Bello MO, et al. 2013. Highly multiplexed single-cell analysis of formalin-fixed, paraffin-embedded cancer tissue. *PNAS* 110:11982–87
115. Lin J-R, Izar B, Wang S, Yapp C, Mei S, et al. 2018. Highly multiplexed immunofluorescence imaging of human tissues and tumors using t-CyCIF and conventional optical microscopes. *eLife* 7:e31657

116. Goltsev Y, Samusik N, Kennedy-Darling J, Bhate S, Hale M, et al. 2018. Deep profiling of mouse splenic architecture with CODEX multiplexed imaging. *Cell* 174:968–81.e15
117. Radtke AJ, Kandov E, Lowekamp B, Speranza E, Chu CJ, et al. 2020. IBEX: a versatile multiplex optical imaging approach for deep phenotyping and spatial analysis of cells in complex tissues. *PNAS* 117:33455–65
118. Schwanhäusser B, Busse D, Li N, Dittmar G, Schuchhardt J, et al. 2011. Global quantification of mammalian gene expression control. *Nature* 473:337–42
119. Payne AC, Chiang ZD, Reginato PL, Mangiameli SM, Murray EM, et al. 2020. In situ genome sequencing resolves DNA sequence and structure in intact biological samples. *Science* 371. <https://doi.org/10.1126/science.aay3446>
120. Eng C-HL, Lawson M, Zhu Q, Dries R, Kouloua N, et al. 2019. Transcriptome-scale super-resolved imaging in tissues by RNA seqFISH+. *Nature* 568:235–39
121. Lee JH, Daugharthy ER, Scheiman J, Kalhor R, Yang JL, et al. 2014. Highly multiplexed subcellular RNA sequencing in situ. *Science* 343:1360–63
122. Wang X, Allen WE, Wright MA, Sylwestrak EL, Samusik N, et al. 2018. Three-dimensional intact-tissue sequencing of single-cell transcriptional states. *Science* 361:eaat5691
123. Stahl PL, Salmen F, Vickovic S, Lundmark A, Navarro JF, et al. 2016. Visualization and analysis of gene expression in tissue sections by spatial transcriptomics. *Science* 353:78–82
124. Liu Y, Yang M, Deng Y, Su G, Enniful A, et al. 2020. High-spatial-resolution multi-omics sequencing via deterministic barcoding in tissue. *Cell* 183:1665–81.e18
125. Lv J, Shi Q, Han Y, Li W, Liu H, et al. 2021. Spatial transcriptomics reveals gene expression characteristics in invasive micropapillary carcinoma of the breast. *Cell Death Dis.* 12:1095
126. Merritt CR, Ong GT, Church SE, Barker K, Danaher P, et al. 2020. Multiplex digital spatial profiling of proteins and RNA in fixed tissue. *Nat. Biotechnol.* 38:586–99
127. Delorey TM, Ziegler CGK, Heimberg G, Normand R, Yang Y, et al. 2021. COVID-19 tissue atlases reveal SARS-CoV-2 pathology and cellular targets. *Nature* 595:107–13
128. Bourgenot C, Saunter CD, Taylor JM, Girkin JM, Love GD. 2012. 3D adaptive optics in a light sheet microscope. *Opt. Express* 20:13252–61
129. Booth MJ. 2014. Adaptive optical microscopy: the ongoing quest for a perfect image. *Light Sci. Appl.* 3:e165
130. Ji N. 2017. Adaptive optical fluorescence microscopy. *Nat. Methods* 14:374–80
131. Royer L, Lemon W, Chhetri R, Wan Y, Coleman M, et al. 2016. Adaptive light-sheet microscopy for long-term, high-resolution imaging in living organisms. *Nat. Biotechnol.* 34:1267–78
132. Krzic U, Gunther S, Saunders TE, Streichan SJ, Hufnagel L. 2012. Multiview light-sheet microscope for rapid in toto imaging. *Nat. Methods* 9:730–33
133. de Medeiros G, Norlin N, Gunther S, Albert M, Panavaite L, et al. 2015. Confocal multiview light-sheet microscopy. *Nat. Commun.* 6:8881
134. Wu Y, Wawrzusins P, Senseney J, Fischer RS, Christensen R, et al. 2013. Spatially isotropic four-dimensional imaging with dual-view plane illumination microscopy. *Nat. Biotechnol.* 31:1032–38
135. Singh SP, Wang L, Gupta S, Goli H, Padmanabhan P, Gulyas B. 2020. 3D deep learning on medical images: a review. *Sensors* 20:5097
136. Dou Q, Yu L, Chen H, Jin Y, Yang X, et al. 2017. 3D deeply supervised network for automated segmentation of volumetric medical images. *Med. Image Anal.* 41:40–54
137. Lu MY, Williamson DFK, Chen TY, Chen RJ, Barbieri M, Mahmood F. 2021. Data-efficient and weakly supervised computational pathology on whole-slide images. *Nat. Biomed. Eng.* 5:555–70
138. Zhou Z-H. 2018. A brief introduction to weakly supervised learning. *Natl. Sci. Rev.* 5:44–53
139. Campanella G, Hanna MG, Geneslaw L, Mirafior A, Silva VWK, et al. 2019. Clinical-grade computational pathology using weakly supervised deep learning on whole slide images. *Nat. Med.* 25:1301–9
140. Lu MY, Chen TY, Williamson DFK, Zhao M, Shady M, et al. 2021. AI-based pathology predicts origins for cancers of unknown primary. *Nature* 594:106–10
141. van der Laak J, Litjens G, Ciompi F. 2021. Deep learning in histopathology: the path to the clinic. *Nat. Med.* 27:775–84

142. Kiemen A, Braxton AM, Grahn MP, Han KS, Babu JM, et al. 2020. In situ characterization of the 3D microanatomy of the pancreas and pancreatic cancer at single cell resolution. bioRxiv 416909. <https://doi.org/10.1101/2020.12.08.416909>
143. Agrawal V, Udupa J, Tong Y, Torigian D. 2020. BRR-Net: a tandem architectural CNN-RNN for automatic body region localization in CT images. *Med. Phys.* 47:5020–31
144. Liu JTC, Glaser AK, Bera K, True LD, Reder NP, et al. 2021. Harnessing non-destructive 3D pathology. *Nat. Biomed. Eng.* 5:203–18